A theoretical modeling framework for motile and colonial harmful algae

Jackie Taylor*[1,2], M. Carme Calderer[3], Miki Hondzo[1,2], and V. R. Voller[1,2]

[1]St. Anthony Falls Laboratory, Minneapolis, Minnesota, USA

[2]Department of Civil, Environmental and Geo Engineering, University of Minnesota, Twin Cities, Minneapolis, Minnesota, USA

[3]School of Mathematics, University of Minnesota, Twin Cities, Minnesota, USA

*Corresponding author: Jackie Taylor, tayl1562@umn.edu

Abstract

1. Harmful algal blooms are increasing in both severity and frequency across the globe. Many bloom-forming species are capable of vertical motility and colony formation. The cyanobacterium *Microcystis aeruginosa* is a common example of such a species, yet current models poorly predict vertical distributions of *M. aeruginosa*.

2. To couple the hydrodynamics, buoyancy, and the colony dynamics of *Microcystis*, we present a system of one-dimensional advection-diffusion-aggregation equations with Smoluchowski aggregation terms.

3. Results indicate Smoluchowski aggregation accurately describes the colony dynamics of *M. aeruginosa*. Further, transport dynamics are strongly dependent on colony size, and aggregation processes are highly sensitive to algal concentration and wind-induced mixing. Both of these findings have direct consequences to harmful algal bloom formation.

4. While the theoretical framework outlined in this manuscript was derived for *M. aeruginosa*, both motility and colony formation are common among bloom-forming algae. As such, this coupling of vertical transport and colony dynamics is a useful step for improving forecasts of surface harmful algal blooms.

Keywords: harmful algal bloom, cyanobacteria, *Microcystis aeruginosa*, aggregation dynamics, vertical motility, theoretical biology

1 Introduction

Microcystis aeruginosa is a common toxin-producing cyanobacterium capable of forming harmful algal blooms (HABs). HABs threaten both ecological and public health, and they are expected to increase in distribution, frequency, and severity as a result of climate change (O'neil et al., 2012). Predicting the timing of bloom formation has been challenging, but experts in the field have reached consensus on general trends leading

up to a HAB. A study of the record-breaking Lake Erie algae bloom of 2011 determined that—in addition to excessive nutrient loading—quiescent meteorological conditions allowed the bloom to form and proliferate to such a massive extent (Michalak et al., 2013), a finding that has been corroborated in many subsequent studies of cyanobacteria HABs (Wells et al., 2015). Using a Bayesian biophysical model with a high-frequency dataset, Del Giudice et al. (2021) were able to quantitatively show that quiescent conditions are not enough: high surface water temperatures and high irradiation are also necessary for bloom formation. Recently, it has been suggested that vertical heterogeneity of *M. aeruginosa* concentration is an important precursor to *Microcystis* surface bloom formation (Seegers et al., 2015; Xiao et al., 2018; Wilkinson et al., 2019). Therefore it is reasonable to assume improving models of *M. aeruginosa* vertical transport will likely lead to improved predictions of HAB timing.

There are two key traits related to the ubiquity of *M. aeruginosa*: vertical motility and colony formation. Vertical motility is achieved through buoyancy regulation via intracellular gas vesicles. Typically, *M. aeruginosa* sinks to lower light intensities during the day and floats towards the water surface at night, although a critical water temperature threshold must be reached in order for cells to regain buoyancy (R. Thomas & Walsby, 1985, 1986). Once that threshold is reached, increasing temperature increases buoyant velocity (You et al., 2018). Vertical motility gives *M. aeruginosa* a particular advantage in stratified lake environments, Stratified lakes are characterized by three distinct layers: the epilimnion or surface mixed layer is the hot, well-mixed surface layer; the hypolimnion is the cold, well-mixed bottom layer; and the metalimnion is the intermediate layer of steep temperature gradient connecting the epilimnion to the hypolimnion. Using the three-dimensional ecological-hydrodynamic modeling software ELCOM-CAEDYM, Chung et al. (2014) were able to demonstrate a shallow mixed layer depth (close to the photic depth) favored buoyant cyanobacteria dominance, indicating lake thermal structure controls algal population dynamics.

Colony dynamics remain rather illusive, but colonies have been demonstrated to form in the presence of grazers, low to medium turbulence, and low nutrient conditions.

Colonies formed by reproduction and growth tend to be compact, whereas colonies that form by collisions tend to be fractal. There is also a well-documented progression from a unicellular morphology in the spring to a fractal colonial morphology in the summer (Xiao et al., 2018). In a field study, Cao and Yang (2010) found that large colonies didn't appear until May, but composed 90% of cells in a June surface bloom. They also calculated the mean number of cells in the surface bloom to be about 120 cells/colony. Between field work and experiments, Qin et al. (2018) found that wind promotes aggregation, creating heterogeneous size distributions in *Microcystis* populations.

There are two threads of previous models to follow. There are models that describe aggregation processes of phytoplankton, and there are models that describe the vertical motility of *M. aeruginosa*. To describe the aggregation processes of phytoplankton, models use Smoluchowski aggregation terms (Smoluchowski, 1917; Jackson, 1990; Ackleh & Miller, 2018). Because these models typically have applications in wastewater treatment or marine snow, the only transport considered is the loss of aggregates via sinking out of the surface mixed layer (Bonner et al., 2000; Teh et al., 2016; Engel et al., 2004). In contrast, *Microcystis* motility models relate individual cell density to light intensity with one-dimensional ordinary differential equations, which are then related to a Stokes velocity (Wallace et al., 2000). Turbulent transport has since been incorporated into these models (Medrano et al., 2013; Zhu et al., 2018). By combining their model with a principal component analysis, Feng et al. (2018) demonstrated that turbulence-induced mixing explained over half of the variability of early surface bloom formation, but buoyancy regulation was more important for bloom maintenance and formation of late-season blooms. Although the transport of different (fixed) colony sizes is investigated in these models, they do not incorporate aggregation dynamics, despite the well-documented progression from unicellular to colonial morphologies.

In a previous field study, statistical methods were used to elucidate the reliance of *Microcystis*-dominated algal vertical distributions on lake thermal stratification variables (Taylor et al., 2021). Following the protocol discussed in Vinatier et al. (2011) which suggests using statistical and mechanistic models in an iterative manner to uncover forc-

84 ings of spatial heterogeneity, we propose a mechanistic model to analyze the effects of
85 hydrodynamic and biological processes underlying the spatial patterns observed in the
86 previous field study. In this paper, we couple the aggregation dynamics with lake hydro-
87 dynamics and algal motility in a system of one-dimensional partial differential equations
88 in an attempt to investigate the role of colony and motility dynamics on *M. aeruginosa*
89 surface bloom formation.

90 2 Methods

91 2.1 Aggregation preliminaries

92 The discrete aggregation dynamics for the concentration of an aggregate of size k, n_k,
93 were described by Smoluchowski (1917) as

$$94 \quad \frac{dn_k}{dt} = \frac{1}{2}\sum_{i+j=k} \alpha(i,j)\beta(i,j)n_i n_j - \sum_{i=1}^{\infty} \alpha(i,k)\beta(i,k)n_i n_k \tag{1}$$

95 where $n_k(z,t)$ is the concentration of an aggregate of size k, $\alpha(i,j)$ is the sticking prob-
96 ability and $\beta(i,j)$ is referred to as the aggregation, or coagulation, kernel of particles of
97 size i and j (Fig. 1). Occasionally the product of $\alpha(i,j)$ and $\beta(i,j)$ is referred to as
98 the aggregation kernel, instead of just $\beta(i,j)$. We leave the two parameters decoupled
99 mainly for the sake of visualizing the process (Fig. 1), but also to conceptually differ-
100 entiate the hydrodynamic drivers of $\beta(i,j)$ (Eqns. 2-5) from the biological drivers of
101 $\alpha(i,j)$ (Section 2.2.2). The first term on the right-hand side describes the formation of a
102 k-sized aggregation, whereas the second term on the right-hand side describes the loss of
103 a k-sized aggregation through the formation of a $k+i$-sized aggregate. An infinitely-sized
104 particle represents a loss of mass due to gelation. Eqn. 1 has had far-reaching applica-
105 tions in addition to phytoplankton modeling, from aerosols to random graph theory and
106 polymerization to planet formation (Aldous, 1999).

107 While analytical solutions exist for some simple aggregation kernels ($\beta(i,j) \sim 1$,
108 $\beta(i,j) \sim i+j$, and $\beta(i,j) \sim ij$), realistic aggregation kernels are rarely analytically

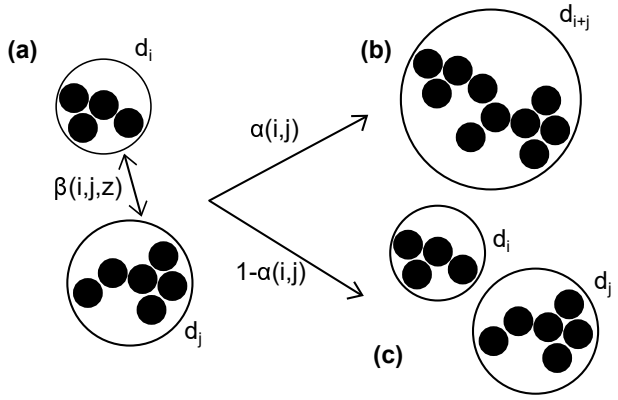

Figure 1: Schematic of aggregation. Circles indicate the equivalent spherical diameter, d_i, of the fractal aggregate of size i. **(a)** Two aggregates of size i and j collide. This collision can either result in **(b)** aggregation and the formation of a $i+j$ sized aggregate, or **(c)** collision without aggregation. Rate of collisions is controlled by $\beta(i,j,z)$, but the number of collisions that result in aggregation is controlled by $\alpha(i,j)$.

tractable. In the present context, $\beta(i,j)$ is calculated as the sum of aggregation kernels for Brownian motion, $\beta_{Br}(i,j,z)$, turbulent shear, $\beta_{TS}(i,j,z)$, and differential settling, $\beta_{DS}(i,j,z)$, each respectively defined as (Ackleh & Miller, 2018; D. Thomas et al., 1999)

$$\beta_{Br}(i,j,z) = \frac{2T(z)k_B\big(d_i + d_j\big)^2}{3\mu(z)\big(d_i d_j\big)} \tag{2}$$

$$\beta_{TS}(i,j,z) = \frac{4G(z)\big(d_i + d_j\big)^3}{3} \tag{3}$$

and

$$\beta_{DS}(i,j,z) = \pi\big(d_i + d_j\big)^2 |w_i(z) - w_j(z)| \tag{4}$$

such that

$$\beta(i,j,z) = \beta_{Br}(i,j,z) + \beta_{TS}(i,j,z) + \beta_{DS}(i,j,z) \tag{5}$$

where $T(z)$ is the water temperature (K), k_B is Boltzmann's constant (1.38×10^{-23} m^2 kg s^{-2} K^{-1}), $\mu(z)$ is the dynamic viscosity of water (kg/m/s), $G(z) = \left(\frac{\epsilon}{\nu}\right)^{\frac{1}{2}}$ is the turbulent shear rate (1/s), $\epsilon(z)$ is the rate of turbulent kinetic energy dissipation (m^2/s^3), and $\nu(z)$ is the kinematic viscosity of water (m^2/s). The equivalent spherical diamater of a colony of size i, d_i (m), is given by

$$d_i = \frac{i^{\frac{1}{D_f}} d_0}{\phi} \tag{6}$$

where $D_f = 2.5$ is the fractal dimension (Nakamura et al., 1993), $d_0 = 5\mu$m is the diameter of a single cell of *M. aeruginosa* (Xiao et al., 2018), and ϕ is the colony porosity that linearly decreases from $\phi = 1$ for single cells and $\phi = 0.2$ for colonies of size k_{max} (Medrano et al., 2013). Eqn. 2 is derived from thermodynamic principles of Brownian motion, Eqn. 3 defines the rate of collisions for sub-Kolmogorov particles in turbulent flow (i.e., the largest aggregate diameter is smaller than the length scale of the smallest turbulent eddies), and Eqn. 4 describes collisions as a result of different-sized aggregates moving at different velocities. Aggregation due to Brownian motion is typically much slower than aggregation due to turbulent shear, and aggregation due to differential settling will be large for aggregates of drastically different sizes but will be small for aggregates of close to the same size.

There are several assumptions of this formulation that should be addressed before continuing. We are assuming diffusion-limited aggregation rather than reaction-limited aggregation, meaning the aggregation process will be limited by diffusion due to Brownian motion and not by the sticking probability of collisions. This is reasonable for colony-forming species of algae in a system where the domain size is much larger than the aggregate sizes. We additionally assume there will be no disaggregation—colonies cannot split up once formed. This assumption is validated by the lab experiments of O'Brien et al. (2004), which demonstrated disaggregation of *M. aeruginosa* is negligible for the size range of aggregates being modeled subjected to expected field turbulence conditions. When aggregates consist of living organisms, it is possible for aggregates to increase in size through cell growth and reproduction in addition to particle collisions. However, it is hypothesized that the fractal colonies of *M. aeruginosa* are formed primarily through collisions, so we neglect aggregation due to cell growth (Xiao et al., 2018). Lastly, in order to facilitate the construction of a one-dimensional model, we assume aggregation is uniform over any given horizontal cross-section.

2.2 The mathematical model

For the sake of generality, we aim to develop a reduced complexity model that (i) circumvents any dynamics not explicitly needed to provide insight into the colony formation processes of *M. aeruginosa*, and (ii) can easily incorporate necessary subroutines and be incorporated into larger routines (Vedder, Ankenbrand, & Cabral, 2021). Let $n_k(z,t)$ be the number of colonies containing k cells of *M. aeruginosa* per unit volume (colonies/m^3), t be time (s), z be depth (m), $D_Z(z)$ be the sum of molecular diffusion and turbulent dispersion coefficients (m^2/s), $w_k(z,t)$ be the buoyant velocity of a colony containing k cells of *M. aeruginosa* (m/s), $\beta(i,j,z)$ be the Smoluchowski aggregation kernel for colonies of size i and j at a depth z defined by Eqn. 5 (m^3/s), and k_{max} be the maximum number of cells in a single colony. If we assume nutrients are not limiting, then we suggest that the combined vertical transport and aggregation of a colony of size k can be described by the following advection-dispersion-reaction equation:

$$\frac{\partial n_k}{\partial t} = \frac{\partial}{\partial z}\left(D_Z \frac{\partial n_k}{\partial z}\right) - \frac{\partial}{\partial z}\Big(w_k n_k\Big) + \frac{1}{2}\sum_{i+j=k} \alpha(i,j)\beta(i,j,z) n_i n_j - \sum_{i=1}^{k_{max}-k} \alpha(i,k)\beta(i,k,z) n_i n_k \tag{7}$$

with boundary conditions

$$\left.\frac{\partial n_k}{\partial z}\right|_{z=0} = \left.\frac{\partial n_k}{\partial z}\right|_{z=h_{max}} = 0 \tag{8}$$

and piecewise uniform initial conditions given by

$$n_k(z,0) = n_k^0(z) = \begin{cases} 2.3 \times 10^7 \text{ colonies/m}^3 & k = 1 \\ 0 & k > 1 \\ 0 & z > h_{ML} \quad \forall k \end{cases} \tag{9}$$

where $z = 0$ at the air-water interface, $z = h_{max}$ at the lakebed, and h_{ML} is the width of the surface mixed layer. The no-flux boundary conditions ensure cells cannot leave the water column through atmospheric or soil exchange. Due to the seasonal progression of

172 *M. aeruginosa* from unicellular to colonial morphology, we begin simulations with only
173 single cells. Since we are typically more interested in overall *M. aeruginosa* concentration
174 profiles rather than the concentration profiles of any given colony size, we must convert
175 concentrations of colonies of size k to total *M. aeruginosa* concentration by

176 $$C(z,t) = \sum_k k n_k(z,t) \tag{10}$$

177 where $C(z,t)$ is the total concentration of *M. aeruginosa* (cells/m^3). Note that we have a
178 discrete number of total cells in the system, but both concentration and time are continu-
179 ous. Using the aforementioned relationships for the aggregation kernel, appropriate form
180 for the sticking probability and diffusion coefficient, and the specification of an expression
181 for the settling velocity, $w_k(z,t)$, we can readily develop a numerical solution of Eqn. 7.

182 ### 2.2.1 System details

183 For *M. aeruginosa*, the largest stable colony size is approximately 320 μm (O'Brien et al.,
184 2004). Meaning for colonies of diameters smaller than 320 μm, we assume fragmentation is
185 negligible for all reasonable environmental conditions. Using the aggregation parameters
186 listed in Section 2.1, this diameter roughly corresponds to a colony of size $k = 580$
187 cells/colony. This would mean Eqn. 7 is a system of 580 PDEs, which is—needless
188 to say—rather computationally expensive. To explore the features of the model in a
189 numerically efficient manner, we have cut off the colony size domain at $k_{max} = 101$
190 cells/colony, which corresponds to a maximum colony diameter of $d_{101} = 160$ μm. This is
191 approximately the mean colony size that Cao and Yang (2010) measured in a *Microcystis*
192 HAB. Further, diameters larger than this size may exceed the Kolmogorov length scale,
193 thereby compromising the validity of Stokes' law and leading to the overestimation of
194 buoyant velocities (Medrano et al., 2013).

195 Recall *M. aeruginosa* typically thrives in stratified lake environments. As such, the
196 model must incorporate depth-dependent water temperature, water density, and turbu-
197 lence profiles. To get a sense of how the model behaves in field conditions, we used

198 data collected by a Self Contained Autonomous MicroProfiler (SCAMP) from Ramsey
199 Lake (45.2073^{o}N, 93.9969^{o}W)—a stratified and eutrophic lake in Minnesota, USA with a
200 history of *M. aeruginosa* blooms (Rao & Hsu, 2008). SCAMP records temperature fluctu-
201 ations throughout the water column. Following the protocol in H.-L. Chen et al. (2001),
202 estimated spectra were calculated using Batchelor curve fitting, which were then used to
203 calculate turbulent kinetic energy dissipation rates. From this dataset, profiles for water
204 temperature, D_Z, and ϵ were constructed from field data under high wind conditions and
205 low wind conditions (Fig. 2). To put these decisions in context, typical values of $\epsilon(z)$ in
206 the field range from 10^{-11} to 10^{-6} m^2/s^3, and typical values of $D_Z(z)$ range from 10^{-6} to
207 10^{-2} m^2/s (Wüest & Lorke, 2003).

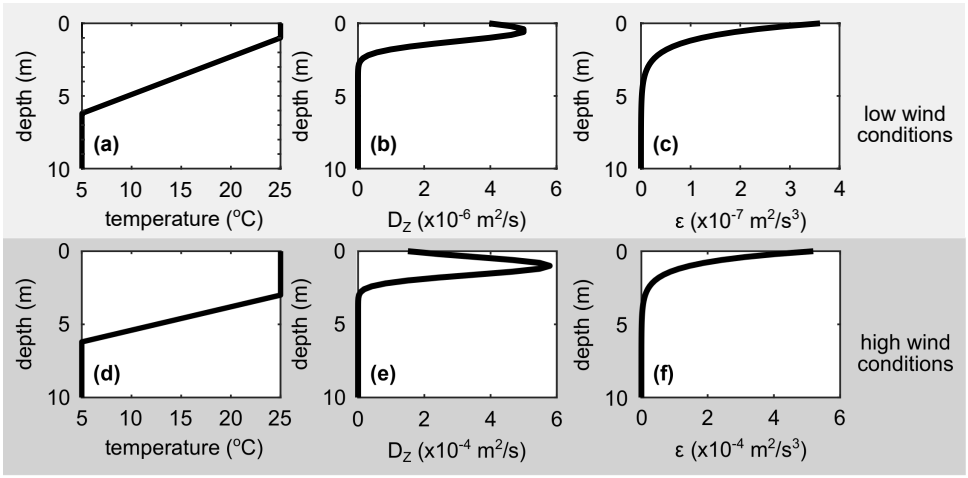

Figure 2: Smoothed field data. Low wind profiles for **(a)** temperature, **(b)** turbulent dispersion coefficient, D_Z, and **(c)** rate of turbulent kinetic energy dissipation, ϵ. High wind profiles for **(d)** temperature, **(e)** turbulent dispersion coefficient, D_Z, and **(f)** rate of turbulent kinetic energy dissipation, ϵ. Note the differences in orders of magnitude for D_Z and ϵ under low wind and high wind conditions.

208 Since *M. aeruginosa* buoyancy is largely mediated by light intensity, we must also
209 construct diurnal light profiles. We generated surface light intensities, $I_0(t)$, by

$$I_0(t) = I_{max} \sin \frac{\pi t}{D_L} \tag{11}$$

210

211 where I_{max} is the maximum surface light intensity and D_L is the photoperiod. To best
212 replicate previous models, values of $I_{max} = 800$ W/m^2 and $D_L = 16$ hours were chosen
213 (Medrano et al., 2013). Depth-dependent light intensities, $I(z, t)$, can then be calculated

214 by

$$I(z,t) = I_0(t)e^{-k_I z} \tag{12}$$

216 where k_I is the light attenuation coefficient ($k_I = 1.3$ m^{-1} (Medrano et al., 2013)).

217 2.2.2 Biological parameters

218 Let us address the sticking probability, $\alpha(i,j)$. Previous models of Smoluchowski aggrega-
219 tion have related $\alpha(i,j)$ to the fractal dimension of aggregates or to the estimated number
220 of particles near the aggregate (Schmitt et al., 2000; Zidar, Kuzman, & Ravnik, 2018).
221 This particularly situation warrants a more biological approach. *M. aeruginosa* uses ex-
222 tracellular polysaccharides (EPS) as adhesive during the aggregation process; therefore,
223 it is reasonable to assume sticking probability will increase with EPS content. Zhu et al.
224 (2014) determined that, in field samples of *M. aeruginosa*, EPS content peaks at colony
225 diameters between 100 and 150 μm. Using this, we define a function that gives the stick-
226 ing probability of a colony of size k, $\alpha_k = f(d_k)$, which achieves a minimum value of
227 $\alpha_k = 0.5$ at $d_1 = 5\mu$m and a maximum value of $\alpha_k = 1$ at $d_{95} = 125\mu$m. To calculate
228 the sticking probability for a collision between a colony of size i and size j, we define
229 $\alpha(i,j) = \max\{\alpha_i, \alpha_j\}$. Larger colonies will therefore be "stickier" than small colonies, so
230 more of their collisions will result in aggregation.

231 The buoyant velocity, w_k, is calculated using subroutines described in previous models
232 which (i) relate light intensity to individual cell density, then (ii) relate individual cell
233 density to colony density using the fractal dimension of *M. aeruginosa* aggregates, then
234 (iii) use the colony density to calculate a modified Stoke's velocity (Wallace et al., 2000;
235 Medrano et al., 2013; Nakamura et al., 1993) by

$$w_k = \frac{g d_k^2 \left(\frac{\rho_k}{\rho_W} - 1\right)}{18\nu} \tag{13}$$

237 where ρ_k is the density of a colony of size k. We expect sinking during the day (positive w_k)
238 and floating at night (negative w_k), although velocity magnitudes and general transport

dynamics will vary across colony size. In experiments, You et al. (2018) recorded buoyant velocities of 10^{-6} m/s at 17.5^{o}C and 10^{-5} m/s at 28^{o}C for small colonies. For large colonies, buoyant velocities have been recorded as large as 10^{-3} m/s (Wallace et al., 2000).

2.2.3 Numerical considerations

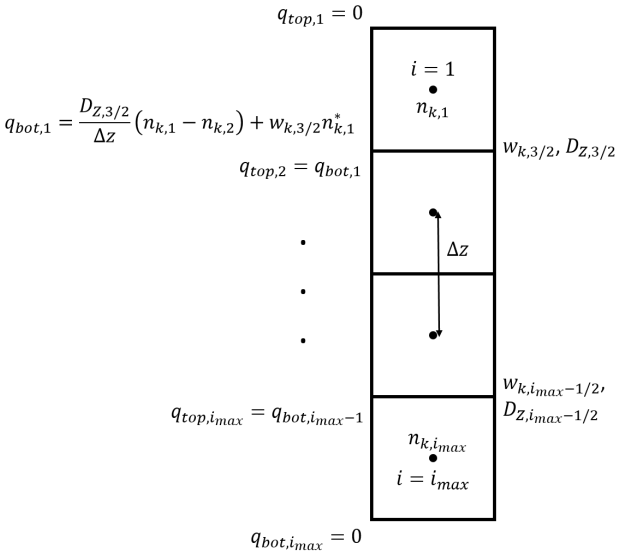

Figure 3: Schematic of numerical scheme. Fluxes, $q_{top,i}$ and $q_{bot,i}$, are calculated as the sum of diffusive and advective fluxes at grid cell interfaces, but concentrations are calculated at grid cell node points. $n^*_{k,i}$ depends on the sign of $w_{k,i}$ and is defined in Eqn. 15. Since we can calculate the new concentration of a colony of size k in grid cell i at time step m by $n^{m+1}_{k,i} = \frac{\Delta t}{\Delta z}(q_{top,i} - q_{bot,i}) + \Delta t$(aggregation terms), conservation of mass is ensured by setting $q_{top,i+1} = q_{bot,i}$. To satisfy boundary conditions, fluxes at the top of the first grid cell and at the bottom of the last grid cell are defined to be zero for all time.

We are using an explicit forward in time upwind numerical scheme with fluxes defined at grid cell interfaces and concentrations defined at grid cell node points (Fig. 3). For a given grid cell i at time step m, the new concentration of colonies of size k in that grid cell is calculated as

$$n^{m+1}_{k,i} = n^m_{k,i} + \frac{\Delta t}{\Delta z}\left(\frac{D_{i-\frac{1}{2}}}{\Delta z}(n^m_{k,i-1} - n^m_{k,i}) + w^m_{k,i-\frac{1}{2}} n^{*m}_{k,i}\right) \ldots$$
$$\ldots - \frac{\Delta t}{\Delta z}\left(\frac{D_{i+\frac{1}{2}}}{\Delta z}(n^m_{k,i} - n^m_{k,i+1}) + w^m_{k,i+\frac{1}{2}} n^{*m}_{k,i+1}\right) + \Delta t(\text{aggregation terms}) \quad (14)$$

where the subscripts $i \pm \frac{1}{2}$ denote parameters defined at the top or bottom interface of grid cell i, the aggregation terms are defined by Eqns. 2-5, and

$$n_{k,i}^{*m} = \begin{cases} n_{k,i-1}^{m} & w_{k,i}^{m} \geq 0 \\ n_{k,i}^{m} & w_{k,i}^{m} < 0 \end{cases} \tag{15}$$

by upwinding.

Table 1 shows numerical parameter values used for all simulations. The time step, Δt, was chosen to be small enough to ensure stability of the numerical scheme, and the grid cell width, Δz, was chosen to be small enough to minimize numerical dispersion of the upwind scheme while also maintaining stability. To address numerical dispersion, we tested the time to large colony appearance for the parameters described in Table 1 against a finer grid size. In the base case simulation, large colonies appear in 13.4 days; if we instead use $\Delta z = 0.1$m (and a correspondingly smaller time step of $\Delta t = 5$s), large colonies appear in 16.1 days. This three day slowdown indicates that our scheme is not completely devoid of numerical dispersion. However, the goal of this manuscript is first and foremost to investigate the applicability of Smoluchowski aggregation to describe *M. aeruginosa* colony dynamics—not to solve the inverse problem of parameter estimation or make predictions with a real data set. In this sense, we feel that our choices of space and time step efficiently capture the correct physical behaviors and provide an appropriate order of magnitude prediction for the timing and appearance of large colony sizes.

Table 1: Numerical parameters.

Variable	Description	Value
Δz	grid cell width	0.2m
Δt	time step	10 s
z_{max}	maximum depth of domain	10 m

Table 2: Base case simulation conditions.

Condition	Description	Further details
motility	regulated by light-dependent buoyancy	Eqn. 13
meteorological forcings	constant high wind and lake thermal profile	Fig. 2d-f
sticking probability	$\alpha(i,j) \in [0.5, 1]$ with peak at $d_{95} = 125\mu$m	Section 2.2.2
initial algal concentration	only single cells in mixed layer	Eqn. 9

3 Results

3.1 Appearance and distribution of colonies

We will start with the simplest simulation that still allows for investigation of important model features: six weeks of a repeating photoperiod and constant lake thermal and hydrodynamic profiles (Table 2). Field data indicate *Microcystis* can transition from a predominantly unicellular morphology to a predominantly colonial morphology over a monthly period, so a six-week simulation time was chosen to ensure aggregation would be evident. Using these conditions, Eqn. 13 predicted buoyant velocities ranging from -10^{-4} (floating) to 10^{-3} m/s (sinking) and Eqns. 2-5 predicted aggregation kernels in the range $\beta(i,j,z) \in [10^{-13}, 10^{-9}]$ m^3/s.

The model demonstrates small colonies will diffuse throughout the mixed layer (Fig. 4a-c), but large colonies exhibit diurnal migrations to a depth with a preferred low light intensity (Fig. 4d-e). In general, small colonies will lose mass as they aggregate into larger colonies, which gain mass. Medium-sized colonies never achieve high mass (Fig. 4c-d), and colonies of size $k = 101$ appear before colonies of size $k = 67$. This indicates large colonies aggregate with each other faster than they aggregate with small colonies, a finding consistent with coagulation kinetic theory (Smit et al., 1994). The overall concentration profile, $C(z,t)$ (Eqn. 10), is mostly influenced by large colonies by approximately the fifth week of simulation (Fig. 4f).

3.2 Factors affecting vertical distribution

While advection is negligible for single cells and small colonies, motility plays a key role in the vertical distribution of large sized colonies (Fig. 5). The time it takes for large

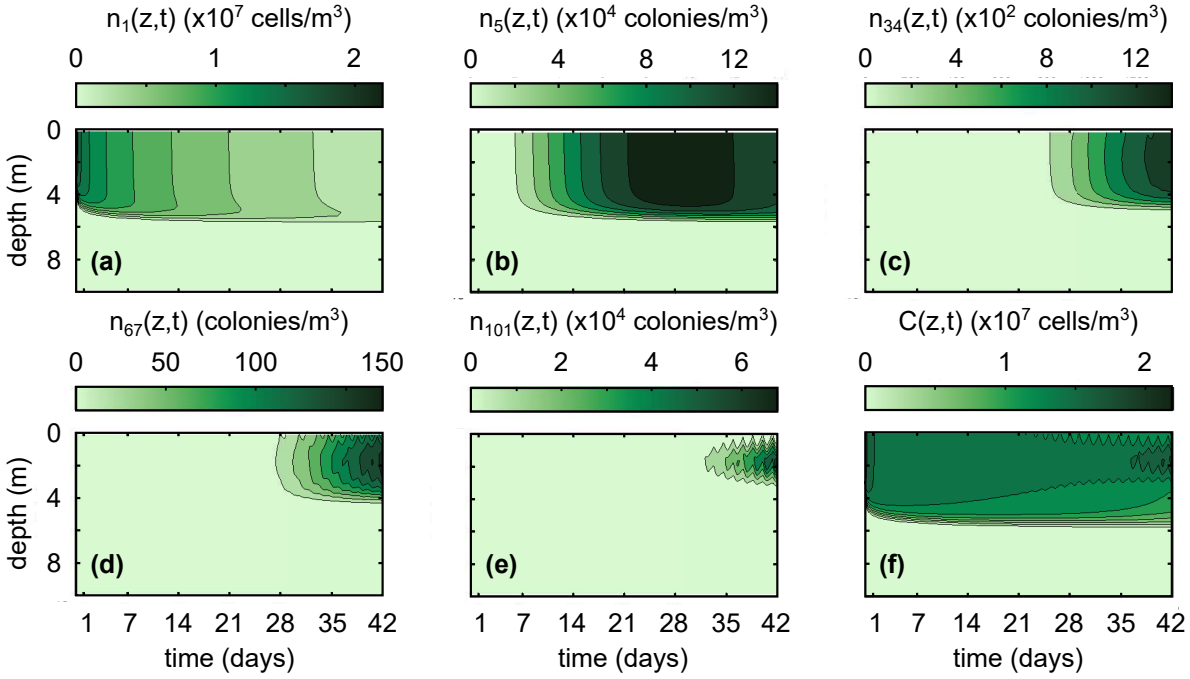

Figure 4: Concentration profiles over six weeks of simulation during high wind conditions (shown in Fig. 2(d)-(f)) for **(a)** $n_1(z,t)$, **(b)** $n_5(z,t)$, **(c)** $n_{34}(z,t)$, **(d)** $n_{67}(z,t)$, **(e)** $n_{101}(z,t)$, and **(f)** $C(z,t)$. Color bar changes scale for each subfigure. The wiggles visible in **(d)**-**(e)** show the diurnal migration of large-sized colonies.

colonies to appear is approximately equivalent whether advection is on or off, but the inclusion of motility allows the large colonies to migrate to a preferred depth of low light intensity (Fig. 5a).

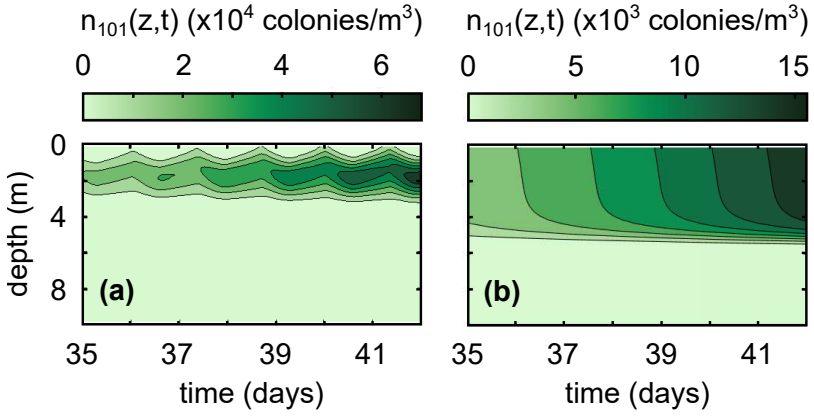

Figure 5: Differences in vertical distributions of large sized colonies between **(a)** the base case simulation in Fig. 4 and **(b)** turning off advection by setting $w_k(z,t) \equiv 0$.

We also see changes in vertical distributions when we change wind conditions (Fig. 6). During high wind conditions, small colonies become uniformly distributed throughout

297 the mixed layer. During low wind conditions, smaller colonies (e.g., $k = 34$) are able to
298 advect to a preferred depth of low light intensity, although their diurnal migrations are
299 not as pronounced (compare Fig. 6b to Fig. 5a or Fig. 4e). In addition, wind also seems
300 to significantly control the time it takes for colonies to appear.

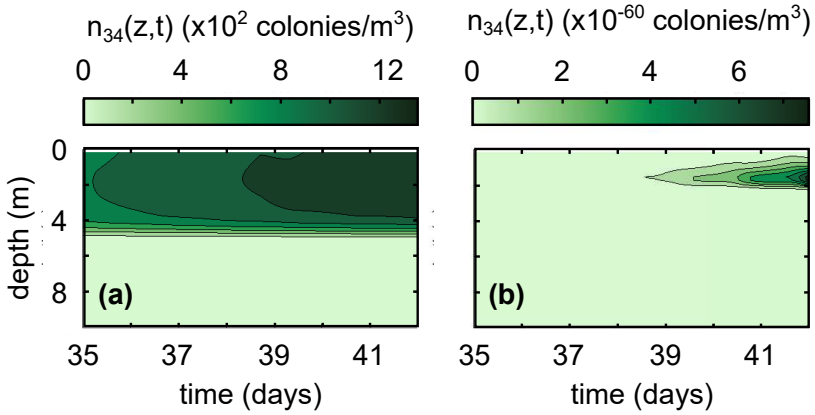

Figure 6: Differences in vertical distributions of colonies of size $k = 34$ between **(a)** the base case simulation in Fig. 4 and **(b)** low wind conditions (Fig. 2).

301 3.3 Factors affecting aggregation

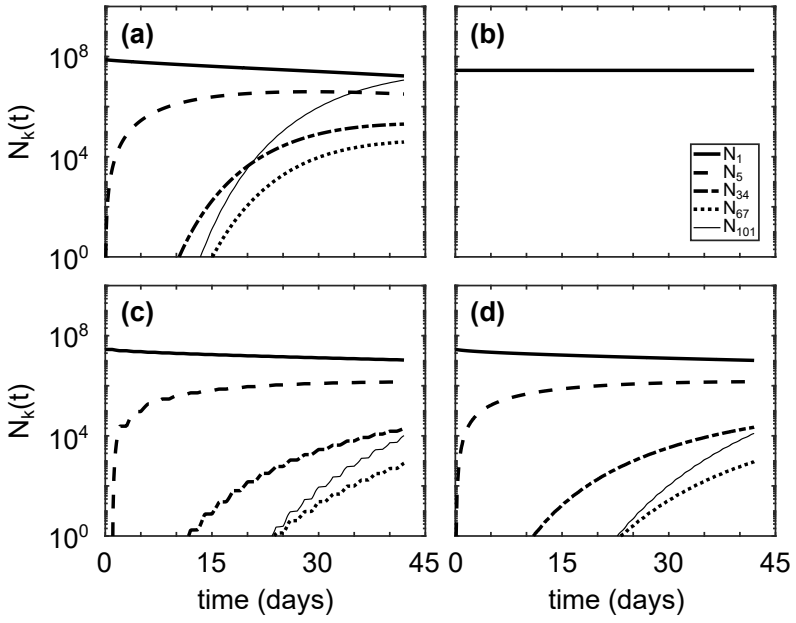

Figure 7: Cell count, $N_k(t)$, of various colony sizes for **(a)** the base case simulation (Table 2), **(b)** low wind conditions (Fig. 2), **(c)** switching between high wind and low wind conditions every day, and **(d)** switching between high wind and low wind conditions every hour. Total number of cells is conserved for all simulations. Cell counts, N_k, were calculated by $N_k = \sum_z k n_k \Delta z$.

There are few situations less likely to occur than six weeks of the exact same meteorological conditions on repeat, so we must explore how the model behaves under different conditions. To this end, let us define

$$N_k(t) = \sum_z k n_k(z,t) \Delta z$$

to be the total number of cells in a colony of size k. Since n_k is a continuous variable and $n_k \Delta z$ is not necessarily greater than one, it is possible for $N_k < k$. We are more concerned when colonies of various sizes appear at some comparative concentration value than the actual concentration, so $N_k(t)$ acts as a suitable marker for appearance of colonies. We can now rerun the simulation described in the previous Section 3.1 while changing one condition at a time to see how each individual change affects $N_k(t)$ for various colony sizes (Figs. 7 and 8). Using low wind conditions (Fig. 2) dramatically reduces aggregation—in the entire six week simulation, the largest colony size achieved is $k = 3$ cells/colony (Fig. 7b). Intermittent wind, either on a daily or hourly time scale, slowed down aggregation by a factor of approximately two (Fig. 7c-d). Setting the sticking probability, $\alpha(i,j)$, to be unity for all colony sizes allows the largest sized colonies to show up approximately five days before their appearance in the base case simulation, eventually becoming more abundant than the single cell population (Fig. 8b).

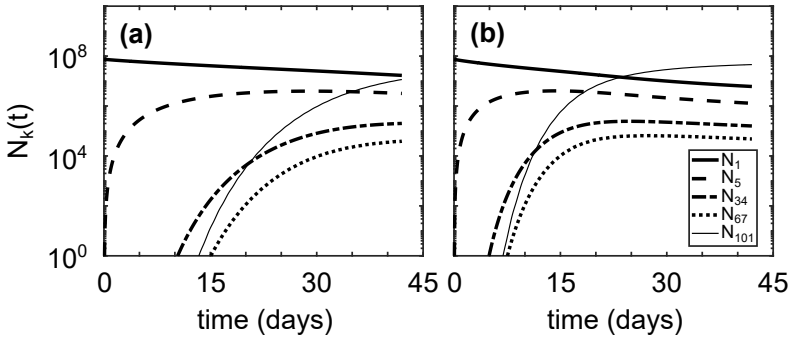

Figure 8: Cell count, $N_k(t)$, of various colony sizes for **(a)** the base case simulation from Fig. 4 and **(b)** enforcing all collisions result in aggregation by setting $\alpha(i,j) \equiv 1$. Total number of cells is conserved for all simulations.

Along with wind conditions, the speed of aggregation is highly sensitive to initial algal concentrations (Fig. 9). Let us define τ_k to be the time such that $N_k(\tau_k) = 1$. As long

as initial algal concentrations are greater than 1×10^7 cells/m^3, then τ_k is approximately inversely proportional to initial concentrations within the mixed layer, n_1^0.

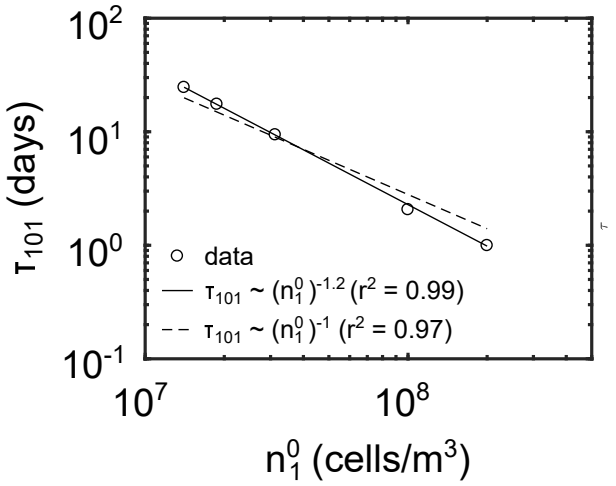

Figure 9: Initial concentration of singles cells within the mixed layer vs time to appearance of colonies of size $k = 101$. Both x- and y-axes are log scale. Solid line shows the best fit, with a slope of -1.2 ($\tau_{101} = 1.1 \times 10^{10}(n_1^0)^{-1.2}$). Dashed lines show an exactly inversely proportional relationship between τ and n_1^0 ($\tau_{101} = 2.7 \times 10^8(n_1^0)^{-1}$). With a starting concentration of 1×10^7 cells/m^3, colonies of size $k = 101$ never appear within the 42-day simulation period.

3.4 Summary of main results

1. For constant high wind conditions and initial uniform single cell concentrations of 10^7 cells/m^3 within the surface mixed layer, colonies of size $k = 101$ appear in approximately two weeks and dominate in approximately five weeks.

2. Large colonies exhibit diurnal migrations, with concentration peaks located around a depth of preferred low-light intensity.

3. Low wind conditions inhibit aggregation.

4. Intermittent wind conditions, which oscillate between high and low winds at some given frequency such that high wind conditions are achieved 50% of the time, slows the appearance of large colony sizes by a factor of two.

5. Above an initial algal concentration of 10^7 cells/m^3, there is a power-law dependence between the time to appearance of large colonies and initial algal concentration.

4 Discussion and conclusion

Our results generally coincide with those of existing literature. Ackleh and Miller (2018) found aggregation rates on the order of 10^{-12} m^3/s using Smoluchowski aggregation to model phytoplankton dynamics, which is in line with those calculated in our simulations ($\beta(i,j,z) \in [10^{-13}, 10^{-9}]$ m^3/s). Our model also predicts aggregation at a time scale that roughly corresponds with the field study by Cao and Yang (2010), wherein the dominant morphology of *Microcystis* transitioned from single cells to large colonies in about a month. The model of Medrano et al. (2013) showed that small colonies of *M. aeruginosa* are not able to overcome turbulent mixing, whereas large colonies exhibit notable daily migrations controlled by the photic depth. This is directly compatible with our model results, keeping in mind that the intensity of wind controls the minimum colony size capable of diurnal migrations (Figs. 4-6). If we define the sticking probability to be unity for all colony sizes, the largest sized colonies appear within a couple days, much faster than they appear in field conditions (Fig. 8). Relating the sticking probability to the extracellular polysaccharide content, which is in turn related to colony size, slows down aggregation to a rate consistent with field observations. These findings support the claim that Smoluchowski coagulation kinetics accurately describe the aggregation processes of *M. aeruginosa*.

The model unveils two important dependencies of aggregation on wind speed and algal concentration. Colony size distributions are highly sensitive to wind-induced mixing (Fig. 7), a phenomenon that was previously revealed in experiments and field work (Qin et al., 2018). Colonies of size $k = 101$ cells/colony appeared within 15 days during high wind conditions, but the largest colony size to appear during low wind conditions was $k = 3$ cells/colony (Fig. 7a-b). Cutting the large wind events in half—either daily or hourly—slowed the appearance of the largest sized colonies by a factor of two (Fig. 7c-d). This implies that the speed of aggregation is directly proportional to the duration of large wind events, causing relatively short-lived wind events to lead to rapid aggregation (recall the dependence of $\beta(i,j,z)$ on the turbulent shear rate in Eqn. 3). This observation has profound consequences on the subsequent formation of surface blooms. Shortly after

large wind events, the newly large colonies will be able to overcome turbulent mixing that the previously small colonies could not, leading to drastically different vertical transport results. Since blooms typically consist of large colonies, this also means short periods of mixing via large wind events could act as a necessary precursor to surface harmful algal bloom formation.

In regards to the sensitivity of aggregation to the initial algal concentration, the inversely proportional relationship between algal concentration and time to large colony appearance, τ_{101}, has been documented in previous studies of marine snow. Jackson (1990) found their largest sized colonies appeared within half a day of algal concentrations reaching 10^8 cells/m^3, a rate in line with the results described in this manuscript (Fig. 9). We relate τ_{101} to initial concentrations only, but that is simply because we have a conserved number of total cells in our system. If instead we had growth and/or decay terms, we could track τ_{101} as a function of instantaneous algal concentration. By maintaining conservation of mass, however, we can clearly see that any location in the water column with algal concentrations on the order of 10^7 cells/m^3 will take over 10 days to form large colonies, whereas locations with concentrations on the order of 10^8 cells/m^3 will have large colonies within a day.

Since higher densities would lead to increased collisions, this finding is unsurprising from a physical standpoint; however, it does provide some important biological modeling insight. Regardless of wind conditions, aggregation will be negligible until algal concentration exceed 10^7 cells/m^3. After this threshold is reached, the rate of aggregation will increase as concentration increases. A large wind event later in the season—when algal concentrations are high—will therefore have dramatically different aggregation consequences than a large wind event in the beginning of the season, when algal concentrations are low. Further, non-uniform algal concentration profiles will lead to non-uniform aggregation. Any depth where there is a peak in algal concentration will also act as a hot spot for aggregation, leading to non-uniform colony size distributions within the water column.

So far we have only discussed the mechanistic insight provided by the model into

the vertical distributions of *M. aeruginosa*, but it is important to remember the ecological consequences of this insight. Surface HABs are mostly comprised of large colonies. Because wind-induced mixing increases the rate of aggregation, we can think of large wind events as a necessary precursor to *Microcystis* bloom formation. Mainstream consensus on cyanobacteria HABs states that quiescent conditions are necessary for bloom formation (Michalak et al., 2013). While this may be true immediately preceding bloom formation, it is also true that there must be enough large wind events before the quiescent period to encourage aggregation in order for a surface bloom to form. But the occurrence of large wind events is still not enough: these wind events must occur when algal concentrations exceed 10^8 cells/m^3 in order for large colonies to form within a day. In addition to modeling concerns, this finding has implications for water quality management. If water samples are taken from well above the photic depth in a lake dominated by motile and colonial cyanobacteria, algal concentrations will likely be low and the average colony size will likely be quite small, which may give the appearance that HAB formation is unlikely. Meanwhile, large colonies could be rapidly forming at subsurface algal concentration peaks near the photic depth, indicating a surface bloom is imminent.

There are many further avenues of study for this model, both from an ecological and numerical perspective. One major ecological concern of *M. aeruginosa* is the ability to produce and release microcystins, a group of toxins that affect the liver. Microcystins are known to increase in extracellular concentration when *Microcystis* is stressed, and they also seem to have a relationship with extracellular polysaccharide content and colony size (Hu & Rzymski, 2019; Li et al., 2020; Rzymski et al., 2020; You, 2020). In fact, it is even hypothesized that microcystins can trigger colony formation via quorum-sensing processes. This raises two important questions: (1) How might the inclusion of microcystin processes improve the performance of this model, and (2) how might this model improve predictions of the spatial heterogeneity of extracellular microcystin concentrations? After all, *M. aeruginosa* is a threat to public health because they release microcystins. In this regard, the fundamental question is not necessarily where the *Microcystis* is, but where the microcystins are.

While this manuscript does not explicitly investigate any temperature dependencies, it is a worthwhile venture as climate change causes global surface water temperatures to warm faster than global air temperatures (Hansen et al., 2010). In experiments, Duan et al. (2018) found that *Microcystis* colony size significantly increased with increasing temperature. Although the aggregation kernel related to Brownian motion scales linearly with temperature (Eqn. 2), this thermodynamic dependency alone cannot explain this variability. For the strains of *Microcystis* being investigated in the experiments, it seems increased algal growth with increasing temperature is responsible for the increase in colony size. In deriving our model, we have previously assumed aggregation due to cell growth is negligible, but this may not be true during peak surface water temperature conditions. To account for cell growth in future iterations of this model, the method of Ackleh and Miller (2018) for calculating cell growth within a colony–where only a certain proportion of cells along the edge of the colony are able to reproduce new cells–should be incorporated into Eqn. 7.

Keeping in mind that the goal is to improve predictions over a seasonal time scale, then it will be necessary to use our model as a subroutine in larger modeling software that can handle hydrodynamics, biogeochemical cycling, and algal life cycles (e.g., AEM3D (Hodges & Dallimore, 2016) or Delft3D-WAQ (Q. Chen & Mynett, 2006)). Since this model demonstrates aggregation is negligible except during high wind events at high algal concentrations, future models could also include a term that switches aggregation off when those conditions are not met. It would also be worthwhile to use these results to instead explore the evolution of the average colony size, $\bar{d}_k$, as a function of algal cell concentration and turbulence intensity. The model proposed in this manuscript is necessary to gain biological and physical insight into algal aggregation processes, but it may be possible to reduce some complexity once the system is understood. Aggregation processes mostly affect buoyant transport, which is governed by the colony diameter-dependent settling velocity described in Eqn. 13. By restructuring the modeling in this way, the system of k equations can be avoided and bulk parameters remain the focus, removing most of the numerical expense that would be added by incorporating Eqn. 7

as a subroutine in software like AEM3D.

While the model described here has been derived for *M. aeruginosa* specifically due to their ubiquity and ecological importance, the modeling framework can easily be applied to any motile and colonial phytoplankton species. Different species have different motility and sticking mechanisms, so calculations of the advective velocity, $w_k(z,t)$, and sticking probability, $\alpha(i,j)$, will need to be tailored to each individual species. *M. aeruginosa* uses intracellular gas vesicles and buoyancy regulation mechanisms to achieve vertical motility, but many species of green algae use flagella to move about the water column, as an example. Despite these differences in subroutine calculations, the theoretical framework will remain largely unchanged from species to species and lake to lake. To promote the use of this model for different algal species, editable and annotated Matlab code used to simulate the base case scenario in Section 3.1 can be found at the Data Repository for the University of Minnesota (DRUM).

In this paper, we have demonstrated that Smoluchowski aggregation accurately represents the colony dynamics of *M. aeruginosa*, and the coupling of transport and colony dynamics is an important feature of *M. aeruginosa* population models in stratified lakes. We have identified ways to (i) incorporate this model into larger software in computationally efficient ways, and (ii) extrapolate this theoretical framework to different algal species. Because *M. aeruginosa* are capable of rapid aggregation during high wind conditions with high algal concentrations, and because large colonies of *M. aeruginosa* behave differently than small colonies for similar hydrodynamic forcings, incorporating colony dynamics into *M. aeruginosa* models has the potential to dramatically improve HAB forecasts in *M. aeruginosa* dominated lakes.

Acknowledgements

The authors wish to thank the Ramsey Lake neighborhood association, the St. Anthony Falls Laboratory engineering and tech support team, Dr. Shahram Missaghi, and Dr. Jiaqi You for help with the Ramsey Lake data acquisition.

Conflict of interest statement

The authors cannot identify any potential conflicts of interest.

Author contributions statement

1. Jackie Taylor developed the model, wrote the code, and wrote the manuscript.
2. Professor M. Carme Calderer provided the mathematical background for the model and provided edits to the manuscript.
3. Professor Miki Hondzo provided the ecological background for the model, analyzed the Ramsey Lake SCAMP data, and provided edits to the manuscripts.
4. Professor Vaughan R. Voller aided with the numerical modeling and provided edits to the manuscript.

Data availability

Data archiving is underway at the Data Repository for the University of Minnesota (DRUM), where interested parties can find lake thermal and hydrodynamic profiles from Ramsey Lake, MN and an example Matlab simulation script.

References

Ackleh, A. S., & Miller, R. L. (2018). A model for the interaction of phytoplankton aggregates and the environment: approximation and parameter estimation. *Inverse Problems in Science and Engineering*, *26*(2), 152–182.

Aldous, D. J. (1999). Deterministic and stochastic models for coalescence (aggregation and coagulation): a review of the mean-field theory for probabilists. *Bernoulli*, 3–48.

499 Bonner, J. S., Garton, L. S., Ernest, A. N., Autenrieth, R. L., et al. (2000). Modeling
500 coagulation kinetics incorporating fractal theories: a fractal rectilinear approach.
501 *Water Research*, *34*(7), 1987–2000.

502 Cao, H., & Yang, Z. (2010). Variation in colony size of microcystis aeruginosa in a
503 eutrophic lake during recruitment and bloom formation. *Journal of Freshwater*
504 *Ecology*, *25*(3), 331–335.

505 Chen, H.-L., Hondzo, M., & Rao, A. R. (2001). Estimation of turbulent kinetic energy
506 dissipation. *Water Resources Research*, *37*(6), 1761–1769.

507 Chen, Q., & Mynett, A. E. (2006). Modelling algal blooms in the dutch coastal waters by
508 integrated numerical and fuzzy cellular automata approaches. *Ecological Modelling*,
509 *199*(1), 73–81.

510 Chung, S.-W., Imberger, J., Hipsey, M., & Lee, H. (2014). The influence of physical
511 and physiological processes on the spatial heterogeneity of a microcystis bloom in
512 a stratified reservoir. *Ecological Modelling*, *289*, 133–149.

513 Del Giudice, D., Fang, S., Scavia, D., Davis, T. W., Evans, M. A., & Obenour, D. R.
514 (2021). Elucidating controls on cyanobacteria bloom timing and intensity via
515 bayesian mechanistic modeling. *Science of The Total Environment*, *755*, 142487.

516 Duan, Z., Tan, X., Parajuli, K., Upadhyay, S., Zhang, D., Shu, X., & Liu, Q. (2018).
517 Colony formation in two microcystis morphotypes: Effects of temperature and
518 nutrient availability. *Harmful Algae*, *72*, 14–24.

519 Engel, A., Thoms, S., Riebesell, U., Rochelle-Newall, E., & Zondervan, I. (2004). Polysac-
520 charide aggregation as a potential sink of marine dissolved organic carbon. *Nature*,
521 *428*(6986), 929–932.

522 Feng, T., Wang, C., Wang, P., Qian, J., & Wang, X. (2018). How physiological and
523 physical processes contribute to the phenology of cyanobacterial blooms in large
524 shallow lakes: A new euler-lagrangian coupled model. *Water research*, *140*, 34–43.

525 Hansen, J., Ruedy, R., Sato, M., & Lo, K. (2010). Global surface temperature change.
526 *Reviews of Geophysics*, *48*(4).

527 Hodges, B., & Dallimore, C. (2016). Aquatic ecosystem model: Aem3d v1. 0 user manual.

Hydronumerics Pty Ltd.

Hu, C., & Rzymski, P. (2019). Programmed cell death-like and accompanying release of microcystin in freshwater bloom-forming cyanobacterium microcystis: From identification to ecological relevance. *Toxins*, *11*(12), 706.

Jackson, G. A. (1990). A model of the formation of marine algal flocs by physical coagulation processes. *Deep Sea Research Part A. Oceanographic Research Papers*, *37*(8), 1197–1211.

Li, Q., Gu, P., Zhang, H., Luo, X., Zhang, J., & Zheng, Z. (2020). Response of submerged macrophytes and leaf biofilms to the decline phase of microcystis aeruginosa: Antioxidant response, ultrastructure, microbial properties, and potential mechanism. *Science of The Total Environment*, *699*, 134325.

Medrano, E. A., Uittenbogaard, R., Pires, L. D., Van De Wiel, B., & Clercx, H. (2013). Coupling hydrodynamics and buoyancy regulation in microcystis aeruginosa for its vertical distribution in lakes. *Ecological Modelling*, *248*, 41–56.

Michalak, A. M., Anderson, E. J., Beletsky, D., Boland, S., Bosch, N. S., Bridgeman, T. B., … others (2013). Record-setting algal bloom in lake erie caused by agricultural and meteorological trends consistent with expected future conditions. *Proceedings of the National Academy of Sciences*, *110*(16), 6448–6452.

Nakamura, T., Adachi, Y., & Suzuki, M. (1993). Flotation and sedimentation of a single microcystis floc collected from surface bloom. *Water Research*, *27*(6), 979–983.

O'Brien, K. R., Meyer, D. L., Waite, A. M., Ivey, G. N., & Hamilton, D. P. (2004). Disaggregation of microcystis aeruginosa colonies under turbulent mixing: laboratory experiments in a grid-stirred tank. *Hydrobiologia*, *519*(1), 143–152.

O'neil, J., Davis, T., Burford, M., & Gobler, C. (2012). The rise of harmful cyanobacteria blooms: the potential roles of eutrophication and climate change. *Harmful algae*, *14*, 313–334.

Qin, B., Yang, G., Ma, J., Wu, T., Li, W., Liu, L., … Zhou, J. (2018). Spatiotemporal changes of cyanobacterial bloom in large shallow eutrophic lake taihu, china. *Frontiers in microbiology*, *9*, 451.

Rao, A. R., & Hsu, E.-C. (2008). Lake temperature data analysis. In *Hilbert-huang transform analysis of hydrological and environmental time series* (pp. 219–233). Springer.

Rzymski, P., Klimaszyk, P., Jurczak, T., & Poniedziałek, B. (2020). Oxidative stress, programmed cell death and microcystin release in microcystis aeruginosa in response to daphnia grazers. *Frontiers in Microbiology*, *11*, 1201.

Schmitt, A., Odriozola, G., Moncho-Jorda, A., Callejas-Fernández, J., Martinez-Garcia, R., & Hidalgo-Alvarez, R. (2000). Multiple contact kernel for diffusionlike aggregation. *Physical Review E*, *62*(6), 8335.

Seegers, B. N., Birch, J. M., Marin III, R., Scholin, C. A., Caron, D. A., Seubert, E. L., … Jones, B. H. (2015). Subsurface seeding of surface harmful algal blooms observed through the integration of autonomous gliders, moored environmental sample processors, and satellite remote sensing in southern c alifornia. *Limnology and Oceanography*, *60*(3), 754–764.

Smit, D., Hounslow, M., & Paterson, W. (1994). Aggregation and gelation—i. analytical solutions for cst and batch operation. *Chemical Engineering Science*, *49*(7), 1025–1035.

Smoluchowski, M. (1917). An experiment on mathematical theorization of coagulation kinetics of the colloidal solutions. *Zeitschrift fur physikalisch Chemie*, *92*, 129–168.

Taylor, J., Hondzo, M., & Voller, V. R. (2021). Abiotic drivers of a deep cyanobacteria layer in a stratified and eutrophic lake. *Water Resources Research*, *57*(6), e2020WR027987.

Teh, C. Y., Budiman, P. M., Shak, K. P. Y., & Wu, T. Y. (2016). Recent advancement of coagulation–flocculation and its application in wastewater treatment. *Industrial & Engineering Chemistry Research*, *55*(16), 4363–4389.

Thomas, D., Judd, S., & Fawcett, N. (1999). Flocculation modelling: a review. *Water research*, *33*(7), 1579–1592.

Thomas, R., & Walsby, A. (1985). Buoyancy regulation in a strain of microcystis. *Microbiology*, *131*(4), 799–809.

586 Thomas, R., & Walsby, A. (1986). The effect of temperature on recovery of buoyancy by
587 microcystis. *Microbiology*, *132*(6), 1665–1672.
588 Vedder, D., Ankenbrand, M., & Cabral, J. S. (2021). Dealing with software complexity
589 in individual-based models. *Methods in Ecology and Evolution*.
590 Vinatier, F., Tixier, P., Duyck, P.-F., & Lescourret, F. (2011). Factors and mecha-
591 nisms explaining spatial heterogeneity: a review of methods for insect populations.
592 *Methods in Ecology and Evolution*, *2*(1), 11–22.
593 Wallace, B. B., Bailey, M. C., & Hamilton, D. P. (2000). Simulation of vertical position
594 of buoyancy regulating microcystis aeruginosa in a shallow eutrophic lake. *Aquatic*
595 *Sciences*, *62*(4), 320–333.
596 Wells, M. L., Trainer, V. L., Smayda, T. J., Karlson, B. S., Trick, C. G., Kudela, R. M.,
597 … others (2015). Harmful algal blooms and climate change: Learning from the past
598 and present to forecast the future. *Harmful algae*, *49*, 68–93.
599 Wilkinson, A., Hondzo, M., & Guala, M. (2019). Investigating abiotic drivers for verti-
600 cal and temporal heterogeneities of cyanobacteria concentrations in lakes using a
601 seasonal in situ monitoring station. *Water Resources Research*, *55*(2), 954–972.
602 Wüest, A., & Lorke, A. (2003). Small-scale hydrodynamics in lakes. *Annual Review of*
603 *fluid mechanics*, *35*(1), 373–412.
604 Xiao, M., Li, M., & Reynolds, C. S. (2018). Colony formation in the cyanobacterium
605 microcystis. *Biological Reviews*, *93*(3), 1399–1420.
606 You, J. (2020). *Growth, motility, and metabolism of harmful cyanobacteria and lipid-*
607 *producing microalgae in fluid environments: from laboratory to field study* (Unpub-
608 lished doctoral dissertation). University of Minnesota, Twin Cities.
609 You, J., Mallery, K., Hong, J., & Hondzo, M. (2018). Temperature effects on growth and
610 buoyancy of microcystis aeruginosa. *Journal of Plankton Research*, *40*(1), 16–28.
611 Zhu, W., Feng, G., Chen, H., Wang, R., Tan, Y., & Zhao, H. (2018). Modelling the
612 vertical migration of different-sized microcystis colonies: coupling turbulent mixing
613 and buoyancy regulation. *Environmental Science and Pollution Research*, *25*(30),
614 30339–30347.

615 Zhu, W., Li, M., et al. (2014). Relationship between extracellular polysaccharide (eps)
616 content and colony size of microcystis is colonial morphology dependent. *Biochem-*
617 *ical Systematics and Ecology*, *55*, 346–350.
618 Zidar, M., Kuzman, D., & Ravnik, M. (2018). Characterisation of protein aggregation
619 with the smoluchowski coagulation approach for use in biopharmaceuticals. *Soft*
620 *matter*, *14*(29), 6001–6012.